BROADBAND IDENTIFICATION OF BATTERY ELECTRICAL IMPEDANCE FOR HEV

R. AL NAZER, V. CATTIN – CEA-LETI, Minatec, Grenoble, France;
P. GRANJON – GIPSA-Lab; M. MONTARU - INES/CEA, France; M. RANIERI. – CEA-LITEN, Grenoble, France

Abstract — Electrical impedance measurements provide useful information about the characteristics of a Li-ion battery. The classical method of measurement consists in performing an impedance spectroscopy relying on offline records of the response of the battery to a controlled current or voltage test signal. This method is robust but presents an important drawback: it is very time consuming, especially for low frequency measurements. In order to overcome this problem and to address embedded applications, we propose to apply broadband excitation signals to perform such impedance measurements. Spectral coherence is an advanced parameter estimated in order to define the frequency bands where the transfer function of a system is accurately identified. The calculation of this parameter can also assess the normalized random errors on both magnitude and phase of the identified impedance since they are related by an explicit mathematical expression. After a brief review of some signal processing tools for identification with broadband excitation signals, we apply this method to identify the impedance of a Li-ion battery and compare performances of various identification patterns on noisy simulated and experimental data.

Keywords— battery impedance, spectroscopy, broadband signals, Li-ion battery, spectral coherence, confidence limits, identification.

I. INTRODUCTION

Thanks to its higher power and energy densities, its long cycle life, low cost of raw materials and superior safety characteristics [1][2], Li-ion battery technology is considered the most attractive for EV and HEV applications, and especially since batteries are their essential component. For reliable operation in these applications, predicting battery performance and service life is thus a significant value to manufacturers as to consumers. Therefore, a Battery Management System (BMS) is always present [3] to measure main battery characteristics like its power fade, and accurately estimate its state of charge (SOC) and state of health (SOH).

Modeling is an essential tool to understand and predict battery behavior. It leads to develop theoretical and practical tools to characterize batteries submitted to different complex electrochemical phenomena. In the literature, various battery models varying from very

detailed electrochemical to high-level stochastic ones have been developed and studied within the framework of a battery state estimator.

Electrochemical models consist of several coupled, non-linear differential equations traducing chemical processes that take place in batteries. [4][5][6] developed an electrochemical model for Li-ion cells. This highly detailed description makes these models the most accurate battery models but at the same time, this approach is complex and difficult to use. Indeed, it requires measurement of many battery internal parameters such as diffusion coefficients, concentration of species in electrolyte, electrode geometry and porosity, transfer coefficient, reaction constant, ... Furthermore, the corresponding measurement experiments can be destructive to the cell.

In analytical models, major properties of batteries are modeled using only few equations. Explicit equations are established to compute battery states. However, such equations are not easy to solve. Peukert's law [7] is an example of such models: it captures the non-linear relationship between battery lifetime and its rate of discharge, but without modeling recovery effect.

Stochastic models have also been used for battery applications. Between 1999 and 2001, Chiasserini and Rao published a series of papers on battery modeling based on discrete-time Markov chains [8][9][10][11]. However, this model is very limited. It focuses only on a specific phenomenon (the recovery effect) and is designed for a specific current profile (pulsed discharge current).

Recently, models based on equivalent electrical circuits became more and more involved in battery applications. It consists of modeling batteries behavior through electrical components. Various physical and chemical processes occurring in a battery are represented by means of passive (resistors, capacitors, inductors) and active (electromotive forces, current sources) electrical elements. Depending on the complexity of the model, this approach describes physical phenomena in batteries but also their overall behavior, and finally highlights the notion of battery electrical impedance. Several studies [12][13][14][15] point out the usefulness of this former quantity as a technique to enhance battery states estimation.

Current embedded methods only estimate the internal resistance of batteries by computing for example the ratio between battery voltage and current during a specific current step [3][16]. In [17], values of equivalent electrical circuit parameters were extracted using impedance measurements made at only three discrete frequencies (2 Hz, 25.18 Hz and 158.9

Hz) based on a mathematical equation system. G. Plett [18] [19] [20] proposed several equivalent electrical circuits more or less complex regarding the precision level required. The principle is to track electrical circuit parameters with different filters depending on the degree of non-linearity of the model to follow. [21] [22] also deals with the use of an extended Kalman filter (EKF) for the observation of parameters of a Li-ion battery lumped model. Nonetheless, the existing EKF algorithm does not account for variations in battery parameters due to electrochemical characteristics modifications caused by aging effect. Therefore, [23] combined the EKF with the per unit system principle to accurately identify battery model parameters and so enhance the SOC and SOH estimation.

Such estimations are strongly limited because they do not represent the wealth of information inherently present in complex and broadband battery electrical impedances. That is the main reason why electrochemical impedance spectroscopy (EIS) is frequently used to better investigate battery states. Its general concept consists in the application of an electrical stimulus to the working electrode, and the monitoring of its corresponding response. Many EIS experiments are performed by a stepwise change of frequency in an applied sinusoidal current, measuring the corresponding sinusoidal voltage and calculating at each frequency the electrochemical impedance (galvanostatic operating mode) [24][25][26].

Concerning the methods mentioned above, each one has its own drawbacks in terms of accuracy, computational complexity, computation time, or compatibility with embedded systems.

The aim of this work is to search for a new technique for measuring battery electrical impedances, that can be easily implemented on BMS for HEV and EV and tends to reduce measurement time. In this paper, we propose to apply broadband excitations. The concept is to measure the system response at multiple frequencies at the same time. Since the measurement time to get a specified accuracy depends on the measurement signal-to-noise ratio (SNR), it is important to select excitations with a high SNR on a wide frequency band. To the author's knowledge, broadband excitation approaches were applied to measure electrochemical impedances in a rather limited number of investigations [27][28][29]. Indeed, advantages of such methods over the conventional single sine excitation methods are not so obvious in the EV community. However, if implemented following a recursive form, they not only allow the reduction of necessary computation time, but also the tracking of battery impedance variations without the need of carrying a new whole measurement. More particularly, [30] explains that the use of broadband signals satisfying specific conditions of

energy transmission in the band of interest can reduce the measurement time, especially in the case of good signal to noise ratio. Undoubtedly, this consideration alone is of significant importance in the context of embedded BMS.

This paper focuses on the test and comparison of broadband excitation signals concerning their performance for battery electrical impedance estimation. Section II recaps non-parametric broadband identification basics for linear and time-invariant systems. The corresponding frequency algorithms are also presented, and their estimation performance is evaluated thanks to advanced spectral quantities such as the spectral coherence. Next, these algorithms are applied to simulated data in section III, where the results obtained with different broadband excitation signals are also compared to each other. Finally, section IV gives experimental results that validate the relevance of this approach.

II. NON PARAMETRIC IDENTIFICATION METHOD

A. LTI Systems

A single input single output (SI/SO) system $\mathcal{H}$ is represented in Figure 1, where $x[n]$ and $y[n]$ are discrete signals verifying Shannon's sampling theorem.

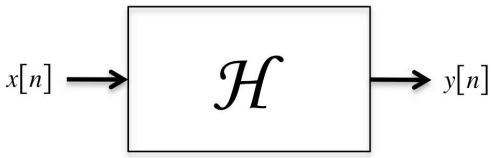

Figure 1. A single input single output system.

If $\mathcal{H}$ is linear and time invariant (LTI), it is completely characterized by its impulse response $h[n]$ or its frequency response function $H(\lambda)$, which are related by a Fourier transform:

$$H(\lambda) = \sum_{n=-\infty}^{+\infty} h[n] e^{-j2\pi\lambda n}. \qquad (1)$$

In this equation, $j = \sqrt{-1}$ and $\lambda \in \left]-\frac{1}{2};\frac{1}{2}\right]$ is the normalized frequency, leading to the frequency f in Hertz when multiplied by the sampling frequency.

Indeed, for periodic deterministic and stationary random signals, input-output relationships in the time and frequency domains are:

$$y[n] = \sum_{k=-\infty}^{+\infty} h[k]x[n-k], \qquad (2)$$

$$S_{yx}(\lambda) = H(\lambda)S_{xx}(\lambda), \qquad (3)$$

where $S_{xx}(\lambda)$ is the power spectral density (PSD) of $x[n]$ and $S_{yx}(\lambda)$ is the cross power spectral density (CPSD) between $x[n]$ and $y[n]$. Eq. (3) gives the frequency domain input-output relationship for a LTI system, and is the foundation of non-parametric identification of such systems in the frequency domain.

B. Non-parametric identification principle

The goal of frequency domain non-parametric identification of LTI systems is to estimate the frequency response function $H(\lambda)$ from input and output measurements without the use of any model.

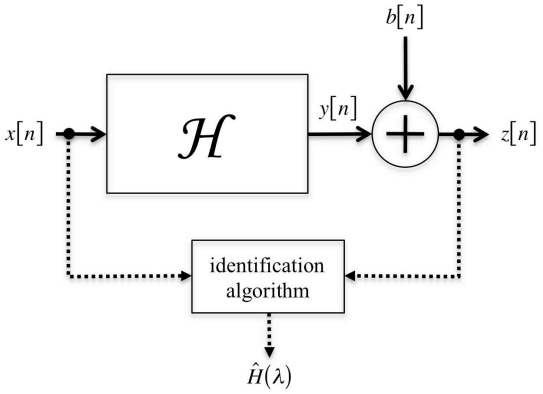

Figure 3. Non-parametric identification of a LTI system $\mathcal{H}$ in the frequency domain.

The general principle of this method is illustrated in Figure 3. A known input signal $x[n]$ is applied to the unknown system $\mathcal{H}$, and a noisy version $z[n]$ of the corresponding output $y[n]$ is measured at the same time. The unknown additive measurement noise $b[n]$ is supposed uncorrelated with $x[n]$ and therefore with $y[n]$. Thanks to this last assumption, Eq. (3) then becomes:

$$S_{zx}(\lambda) = S_{yx}(\lambda) = H(\lambda)S_{xx}(\lambda). \qquad (4)$$

Therefore, on the frequency bands where the input PSD $S_{xx}(\lambda) \neq 0$, the unknown frequency response function $H(\lambda)$ can be calculated through:

$$H(\lambda) = \frac{S_{zx}(\lambda)}{S_{xx}(\lambda)} \text{ if } S_{xx}(\lambda) \neq 0. \qquad (5)$$

This finally leads to the frequency domain identification of the unknown system $\mathcal{H}$. Eq. (5) clearly shows that it is advantageous to use broadband input signals $x[n]$ since they allow the computation of $H(\lambda)$ on a wide frequency band as a whole.

An essential quantity in such a method is the spectral coherence between measured signals $x[n]$ and $z[n]$ [31][32]:

$$|c_{zx}(\lambda)|^2 = \frac{|S_{zx}(\lambda)|^2}{S_{xx}(\lambda)S_{zz}(\lambda)}. \qquad (6)$$

This statistical quantity is bounded by 0 and 1, and measures the linear dependency or correlation between $x[n]$ and $z[n]$ at each frequency λ [31][32]. Moreover, it also can be interpreted as a LTI system detector between $x[n]$ and $z[n]$ [33]. In case of Figure 3, $|c_{zx}(\lambda)|^2$ becomes:

$$|c_{zx}(\lambda)|^2 = \frac{S_{yy}(\lambda)}{S_{yy}(\lambda) + S_{bb}(\lambda)} = \frac{\text{SNR}_\text{o}}{1 + \text{SNR}_\text{o}}, \qquad (7)$$

where $\text{SNR}_\text{o} = \frac{S_{yy}(\lambda)}{S_{bb}(\lambda)}$ is the output signal to noise ratio quantifying the additive noise $b[n]$ relative to $y[n]$. Eq. (6) and (7) can be interpreted as follows:

- when $|c_{zx}(\lambda)|^2 \to 1$, $x[n]$ and $z[n]$ are strongly correlated and $\text{SNR}_\text{o} \to +\infty$ at λ. In that case, $b[n]$ is negligible compared to $y[n]$ and the LTI model for the unknown system $\mathcal{H}$ is totally justified around this frequency;
- when $|c_{zx}(\lambda)|^2 \to 0$, $x[n]$ and $z[n]$ are uncorrelated and $\text{SNR}_\text{o} \to 0$ at λ. This corresponds to an important measurement noise $b[n]$ dominating the system output $y[n]$. In that case, the LTI model of $\mathcal{H}$ cannot be justified as easily around this frequency.

Another interesting property of the spectral coherence is that it is closely related to estimation errors obtained when identifying $H(\lambda)$. This is used in the following to compute confidence limits for different spectral estimators.

C. Non-parametric identification algorithm

Eq. (5) and (6) show that PSD and CPSD are necessary to compute the desired frequency response function and spectral coherence. Such quantities can easily be estimated through the well-known Welch modified periodogram [32]. Measured signals are first split-up into L data segments of length N. All these segments are then windowed by a window function $w[n]$ of length N, and the Fourier transform of each windowed segment is computed by the use of the discrete Fourier transform and fast Fourier transform algorithm. Finally, products of these Fourier transforms are averaged in order to estimate the desired spectral quantities. As an example, the corresponding estimator of the CPSD between $x[n]$ and $z[n]$ is given by:

$$\hat{S}_{zx}(\lambda) = \frac{A}{L}\sum_{k=0}^{L-1} Z_k(\lambda) X_k^{*}(\lambda), \qquad (8)$$

where:

- A is a normalization factor,
- $Z_k(\lambda)$ (resp. $X_k(\lambda)$) is the Fourier transform of the k^{th} windowed segment of $z[n]$ (resp. $x[n]$),
- * denotes the complex conjugate.

Similarly, the estimator of the PSD of $x[n]$ $\hat{S}_{xx}(\lambda)$ is obtained by replacing $Z_k(\lambda)$ by $X_k(\lambda)$ in Eq. (8).

Simple estimators can now be obtained to estimate the spectral coherence $|c_{zx}(\lambda)|^2$ and the frequency response function $H(\lambda)$ by using Eq. (8) in Eq. (5) and (6):

$$|\hat{c}_{zx}(\lambda)|^2 = \frac{|\hat{S}_{zx}(\lambda)|^2}{\hat{S}_{xx}(\lambda)\hat{S}_{zz}(\lambda)}, \qquad (9)$$

$$\hat{H}(\lambda) = \frac{\hat{S}_{zx}(\lambda)}{\hat{S}_{xx}(\lambda)} \text{ if } \hat{S}_{xx}(\lambda) \neq 0. \qquad (10)$$

The last relation also allows estimation of the gain $\hat{G}(\lambda) = |\hat{H}(\lambda)|$ and phase $\hat{P}(\lambda) = \arg\{\hat{H}(\lambda)\}$ of the frequency response function $H(\lambda)$. Moreover, it has been shown in [32], [34] and [35] that under general conditions, the variance of these two estimates is directly related to the spectral coherence by the following expressions:

$$\mathrm{var}\left\{\hat{P}(\lambda)\right\} = \mathrm{var}\left\{\ln\left(\hat{G}(\lambda)\right)\right\} = \frac{1}{2L}\frac{1-\left|c_{zx}(\lambda)\right|^2}{\left|c_{zx}(\lambda)\right|^2}. \quad (11)$$

This interesting result shows two important things. First, estimation errors of the frequency response function are inversely proportional to the number of data segments L used in the Welch estimator of Eq. (8). Second, estimation errors are closely related to the spectral coherence and more precisely, the higher the spectral coherence, the smaller the estimation errors. Eq. (11) has been used in [34] to compute upper and lower 95% confidence limits for the gain and phase estimates $\hat{G}(\lambda)$ and $\hat{P}(\lambda)$ by replacing the true spectral coherence $\left|c_{zx}(\lambda)\right|^2$ by its estimated value $\left|\hat{c}_{zx}(\lambda)\right|^2$:

$$\log_{10}\left\{\hat{G}(\lambda)\right\} \pm 1.96\sqrt{\frac{\left(\log_{10}(e)\right)^2}{2L}\frac{1-\left|\hat{c}_{zx}(\lambda)\right|^2}{\left|\hat{c}_{zx}(\lambda)\right|^2}} \quad (12)$$

$$\hat{P}(\lambda) \pm 1.96\sqrt{\frac{1}{2L}\frac{1-\left|\hat{c}_{zx}(\lambda)\right|^2}{\left|\hat{c}_{zx}(\lambda)\right|^2}} \quad (13)$$

Finally, Eq. (8) and (10) constitute the "identification algorithm" appearing in Figure 3 and used to estimate the frequency response function $H(\lambda)$ of an unknown LTI system through its input $x[n]$ and noisy output $z[n]$. Eq. (9), (12) and (13) are used to evaluate the algorithm performance by computing 95% confidence limits of the previous estimators.

In what follows, batteries are modeled as electrical LTI systems whose input is their current and whose output is their voltage. This choice is based on practical considerations, since control of current and measurement of voltage stages of a battery are already present in currently developed BMS The corresponding frequency response function is then the electrical impedance of the battery, and this quantity is estimated thanks to the previous set of equations.

III. BROADBAND IDENTIFICATION OF ELECTRICAL IMPEDANCE FOR LI-ION BATTERIES

A. Battery modeling

In this study, modeling a battery aims to reproduce its electrical behavior through an equivalent electrical circuit (EEC) [36]. These models, the so-called gray box models,

reproduce the dynamic behavior of batteries basing oneself on an analogy between physicochemical phenomena and common electrical or nonelectrical elements. For electrical engineers, such a model is common to characterize electrochemical phenomena, and leads to perform a quick analysis and prediction of the battery behavior in frequency as in time domains [37].

Many electrochemical studies focus on fine association between impedance spectrum parts and fundamentals physicochemical processes. Some authors [38][39][40][41] consider that the anode effects appear in high frequencies more than in low ones, while the cathode reacts more in low frequencies. Randles [42] proposed an electrical equivalent circuit based on physicochemical processes. It includes the modeling of connectors and electrolyte (R,L), charge transfer (R_{tc}) and double layer (C_{dl}) phenomena [43]. The open circuit voltage (OCV) depends on current intensity and battery SOC, and can be tabulated thanks to a look-up table. Finally, the diffusion phenomenon is modeled by Warburg impedances [43]. Usually, constant phase elements (CPE) are introduced to accurately reflect the behavior of the battery observed through impedance spectroscopy measurements [44][45]. For Li-ion batteries, an additional electrochemical process is observed: the passivation film [46][47]. [48][49][50][51] suggest to model this latter process by a R_f // CPE_f cell. Buller [48] and Moss [51] consider that the first semi circle associated to passivation film does not depend on the current intensity and slightly varies with the SOC. Based on those ascertainments, K. Dong [37] proposed to use an adapted Randles circuit (Figure 4) that we adopt in our study. In his work, he demonstrates an excellent fitting between measured impedance spectra of a graphite/LiFePO4 battery and this model under specific operating conditions, like limited temperature range and frequency band allowing disregard of voltage-contribution associated to diffusion processes.

Finally, a non-linear optimization method is used to estimate the value of each EEC parameter from the measured electrical impedance. In [52], we address uniqueness issue of this inverse problem and propose an efficient two steps optimization approach to improve convergence rate and accuracy. A statistical study was performed and has revealed that this new algorithm presents a very good convergence rate, and leads to unbiased estimates of model parameters. Experimental data has also been used to validate this new approach. The corresponding EEC parameters obtained thanks to this algorithm for a SOC of 60% and a polarization discharge current of 1A are given in **Erreur ! Source du renvoi introuvable.**.

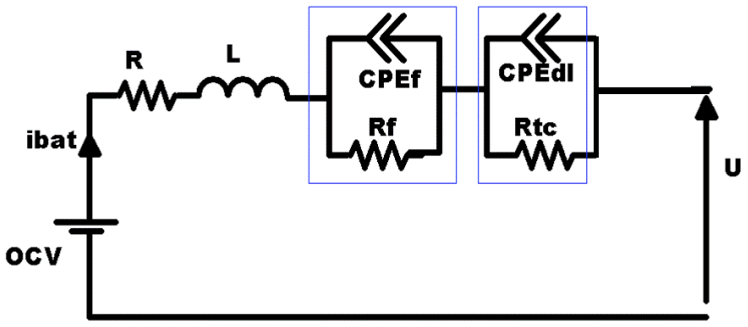

Figure 4. Equivalent electrical circuit (adapted Randles model) of a graphite/$LiFePO_4$ battery.

R (Ohm)	0.0128
L (H)	$4x10^{-8}$
R_f (Ohm)	0.0047
CPE_f: (T_f,P_f)	(5.7, 0.5)
R_{tc} (Ohm)	0.0244
CPE_{dl}: (T_{dl}, P_{dl})	(740, 0.65)

Table 1: EEC parameters numeric values for a SOC of 60% and a polarization discharge current of 1 A.

B. Spectroscopy

Electrochemical spectroscopy [48] commonly used in laboratory consists of exciting the battery with a small sinusoidal current $i(t)$ of frequency f, $i(t) = I_{\max} \sin(2\pi f t)$, superimposed to a DC current, and measuring its voltage response $v(t) = V_{\max} \sin(2\pi f t - \varphi)$ [53]. Therefore, the voltage/current ratio in the frequency domain is expressed as a complex impedance:

$$Z_{est}(f) = \frac{V_{\max}}{I_{\max}} * \exp(-j\varphi) \qquad (14)$$

Though robustness and precision of the results, electrochemical spectroscopy is not suitable for EV and HEV applications due to several reasons. Firstly, an expensive complex electronic is needed to generate sine waves. Secondly, a large frequency band scan with fine frequency resolution takes a long time to be completed, especially when systems with large time constants are studied since it is necessary to wait until transients disappeared after each frequency step. Finally, for embedded system (particularly for EV and HEV applications in this work) where the battery impedance evolves and the BMS should track the impedance evolutions: the use of the EIS technique impose a new whole measurement to get an online estimation. An alternative solution based on broadband identification techniques presented in section II is proposed in what follows.

C. Broadband excitation signals

The selection of optimal excitation signals is an important step in the design of the embedded system. Section II. has shown that in order to estimate the whole electrical impedance at once, they should be able to excite the system with an almost flat power spectrum in the frequency band of interest. This is the main reason why sine waves should be avoided for this application. In this section, broadband signals are introduced as identification patterns that can be used to overcome the spectroscopy drawbacks noticed above. We consider five broadband signals frequently used in system identification applications: white noise, pseudo random binary sequences (PRBS), swept sine, swept square and a square wave [30]. The fifth signal is not on itself a broadband signal but can be considered so if its harmonics are in the frequency band of interest. Such signals allow the estimation of the frequency response function of LTI systems, in particular battery impedances, over a large bandwidth from a single set of measures. Thus operating conditions with broadband signals to assume that the battery follow LTI hypotheses are less tough that those imposed by EIS.

1) Random white noise

A white noise presents a flat power spectrum over all frequencies. Moreover, we filter it in order to inject power only in the frequency band of interest [30].

2) Pseudo random binary sequence

PRBS is a deterministic periodic sequence of length N that switches between two levels +A and –A. Using n_r registers, a sequence of length $N = 2^{n_r} - 1$ can be generated. And by choosing the time for a bit T_b, the highest frequency that will be excited is $f_{max} = 1/T_b$ while the lowest one is $f_{min} = f_{max}/n_r$. PRBS presents an almost flat power spectrum over the frequency band $[f_{min}, f_{max}]$ [30].

3) Swept sine

Also called periodic chirp, it is a sine whose frequency is swept up and/or down from one period to another. A logarithmic variation of frequency (from f_{min} to f_{max}) with respect to time is chosen. An almost flat spectrum is also provided over the frequency band $[f_{min}, f_{max}]$ [30].

4) Swept square

Similarly to the swept sine, this is a square with a logarithmic sweep of its fundamental frequency in the band $[f_{\min}, f_{\max}]$.

5) Square

Though a square is not precisely a broadband signal, by a correct choice of its fundamental frequency, one can use the frequencies that correspond to its odd harmonics to excite several discrete frequencies in the band of interest.

In order to get a better understanding of the nature of the former signals, we compare each other using their PSD, estimated through Eq. (8). As an example, we focus on the frequency band from 136 Hz to 819 Hz. All the signals have a total time duration of approximately 160 seconds, and the sampling frequency f_s is 8190 Hz. These signals are split-up into L=2059 disjoint segments of length N=630 samples. Consequently, each segment has a time duration of $T = N/f_s$ =0.0769 seconds, which results in a frequency resolution of $1/T$ =13 Hz. This former quantity should be chosen so that it is possible to distinguish two consecutive harmonics of the square wave. Moreover, Eq. (11) indicates that the number of data segments L should be chosen as large as possible in order to minimize the estimation error of the electrical impedance. The five resulting PSDs are shown in Figure 6. Under assumption of constant power for the excitation signals, we note that the spectral information is different concerning levels and frequency bandwidths.

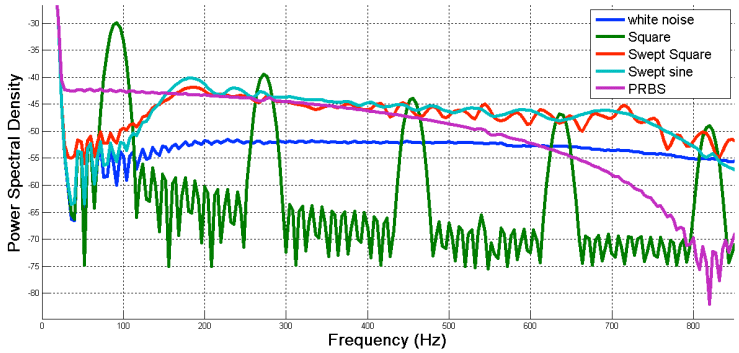

Figure 6. PSD of the five excitation signals.

D. Simulink simulator

The analytical expression of the impedance can be computed from the EEC of Figure 4 and is taken as the theoretical value to estimate. This quantity is a function of the SOC and the

intensity of the DC current. The implementation in Simulink of this model simulates the behavior of a graphite/$LiFePO_4$ battery supplied with a given input current composed, in our case, of a DC current added with one of the broadband signals previously described.

In the context of the non-parametric identification method presented in section II., the system must be LTI during the whole measurement time. Therefore, this condition should also be respected during simulations. It forces to limit the time duration of the excitation signals so that according to the DC current level, there is only a little variation of the battery state of charge. Consequently, we chose a time duration that does not load or unload the battery from over 2% (value usually considered for EIS). This time constraint has two consequences on the proposed method: firstly it is difficult to excite the battery with very low frequencies under high DC currents since in that case, the whole measurement time has to be very short; secondly, it limits the number L of data segments and can increase eventual estimation errors.

The simulations are undertaken under the same operating conditions of SOC (60%) and DC current (1A), and the same values as those given in section III.C are chosen (L=2059, N=630, f_s=8190Hz, T=0.0769s). To simulate an additive measurement noise, a white Gaussian noise with zero mean and several levels of variance is added on the output voltage signal. Spectral coherences and electrical impedances are then estimated from this noisy voltage and the excitation signals through Eq. (9) and (10). Estimated electrical impedances are finally compared to the theoretical impedance value in order to evaluate the quality of the identification process.

E. Coherence results

We first consider a reasonable measurement noise of SNR=0 dB in the next two sections. Figure 8 shows the coherences estimated with the five excitation signals previously defined, and it can be clearly noticed that the results are different even though excitation signals are designed to excite the same frequency band.

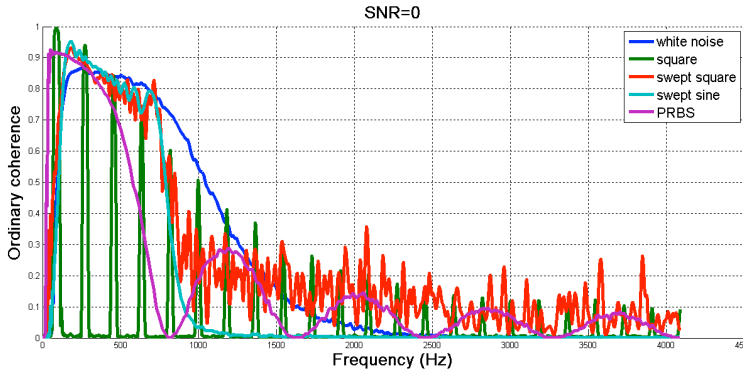

Figure 8. Coherence plots for the five excitation signals with a measurement SNR=0 dB.

Though the white noise preserves a high coherence value over the excited frequency band, it is difficult to generate with a simple electronic and thus cannot be used in our application. The PRBS is able to excite frequencies lower than the low-limit of the selected band $f_{\min}$, and injects less power in the frequencies near the upper limit $f_{\max}$. This could be useful when the aim of the measurement is to estimate the electrical impedance around the lowest frequencies of the selected band. Although other signals can be designed to excite low frequencies, by the use of a PRBS, a better estimate is obtained near $f_{\min}$ with the same time duration. Swept square and swept sine roughly present the same behavior upon the frequency band of interest. For these two excitation signals, the coherence slightly decreases with the frequency, but they still inject more power than the PRBS in the frequencies close to $f_{\max}$. It can also be noted that due to its harmonics, swept square weakly excites frequencies beyond the selected band. This could be useful to find information localized at high frequency. As expected, the coherence obtained with the square wave is only significant at its fundamental frequency and its odd harmonics.

To touch upon some applications where these signals are useful, one can remind that literature assumes that SOC is estimated using information contained in lower frequencies, while the SOH is tied to higher frequencies. Hence, PRBS could be suitable for SOC estimation while swept square is more dedicated to SOH estimation. Besides, another approach can be proposed: to identify impedance only on several discrete frequencies and to fit a model to build the whole frequency response. This approach can be addressed with a square signal, providing that the fundamental frequency and its first harmonics tie to the selected frequencies of interest.

F. Confidence limits results

Confidence limits upon gain and phase factors quantify the estimation performance reached by this identification method and can be easily computed by using Eq. (12) and (13). In this section, the results concerning the gain factor are given as an illustrative example, and they are exclusively represented in the selected frequency band. Results concerning the phase factor are very similar.

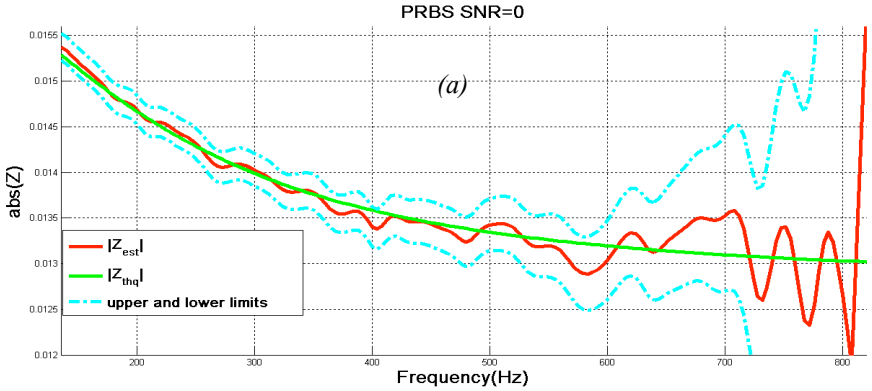

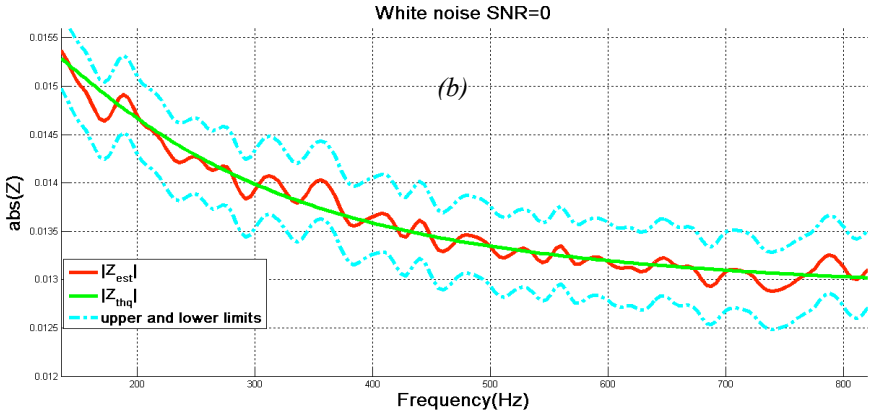

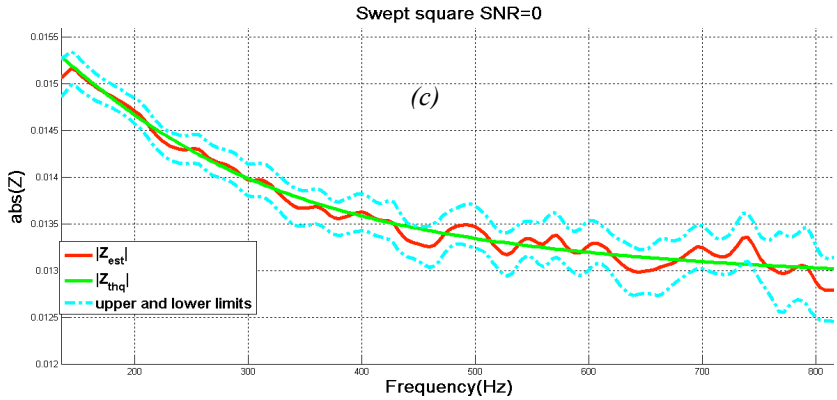

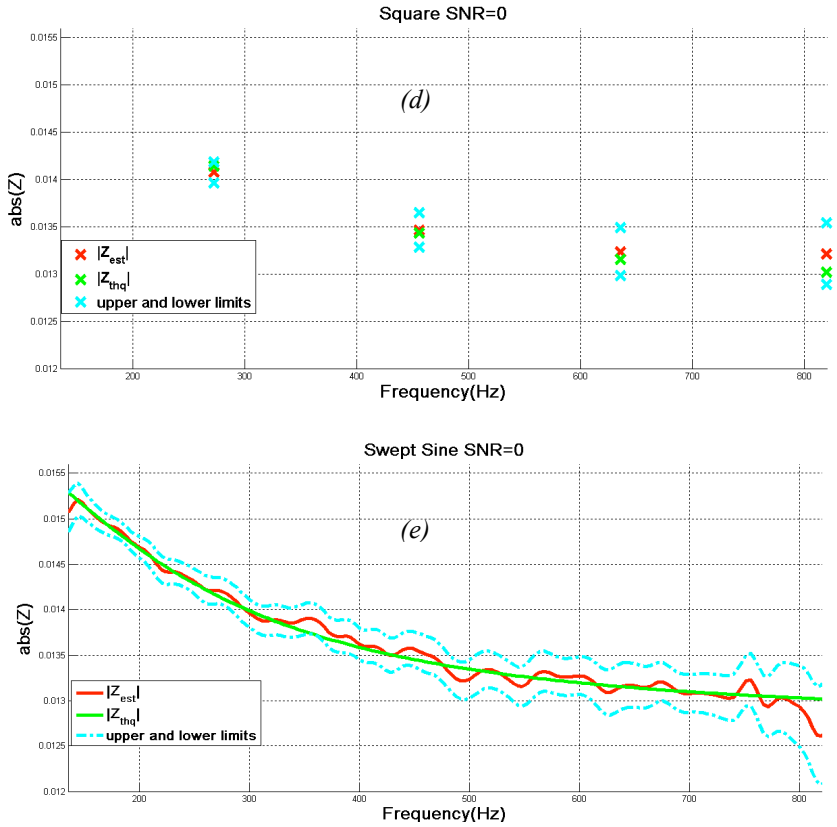

Figure 10. 95% confidence limits results using: (a) PRBS, (b) white noise, (c) swept square , (d) square, (e) swept sine as excitation signals with a measurement SNR=0 dB.

The different subfigures of Figure 10 show that the PRBS (Figure 10(a)) has large confidence limits near the upper limit of the band $f_{\max}$, which confirms the coherence results of Figure 8. Moreover, tight confidence limits are observed upon the whole selected frequency band using a white noise (Figure 10(b)), a swept square (Figure 10(c)) or a swept sine (Figure 10(e)). The square wave (Figure 10(d)) provides, as expected, tight confidence limits only around its odd harmonics frequencies.

We infer from those results that broadband impedance can be identified with signals composed of square patterns (PRBS, swept squares and square waves) with as good quality as classical signals (white noise and swept sine). Such signals are easy to apply to a battery from simple electronic components, for example by using electronic switches. Therefore, we only consider in the next sections square waves, swept squares and PRBS.

G. Noise effect

The above results were presented with a simulated voltage measurement noise such that SNR=0 dB. In this section, we study the effect of this noise by varying the level of its variance.

It is obvious that the measurement noise affects the coherence function: the higher the noise variance, the lower the coherence value. Besides, as the coherence decreases with the noise variance, the confidence limits become larger and the identification performance finally decreases. These effects could be removed by increasing the number of averaging blocks L. However, such an operation will increase the time duration of the measurements, and may modify the system state by loading or unloading the battery of more than 2%. The hypothesis of a LTI system may thus be wrong. Therefore, in the present study, the length of the different signals remains the same whatever the noise quantity.

To study the noise influence, a statistical study is performed. For each SNR level, we simulate $r = 100$ realizations of the output additive noise, and we plot the mean squared estimation error in % (Figure 11) defined by Eq. (15). This error quantifies the averaged normalized difference between the estimated impedance $\hat{z}$ and its theoretical value z over the selected frequency band and for a specific excitation signal.

$$\begin{aligned} Error(k) &= \underset{f}{\text{mean}}\left[\frac{\left|\hat{Z}(k,f) - Z(f)\right|^2}{\left|Z(f)\right|^2}\right], \\ MSE_{\%} &= 100 \times \underset{k}{\text{mean}}\left(Error(k)\right) \end{aligned} \qquad (15)$$

where $\hat{Z}(k,f)$ is the estimated electrical impedance with the k^{th} noise realization.

We first note that the identification performance obtained with the three chosen input signals presents the same behavior as the SNR varies. Indeed, each error decreases when the measurement noise decreases. Moreover, estimation error obtained with a PBRS is always higher than error obtained with swept squares and square signals. This is coherent with the results previously obtained on confidence limits. Finally, this identification method reaches very good estimation performance as soon as the output SNR is higher than or equal to 0 dB, since whatever the excitation signal, the estimation error is then lower than 1%.

In the following section, the proposed identification method is experimentally applied to a battery cell in order to validate the proposed method and the previous simulation results.

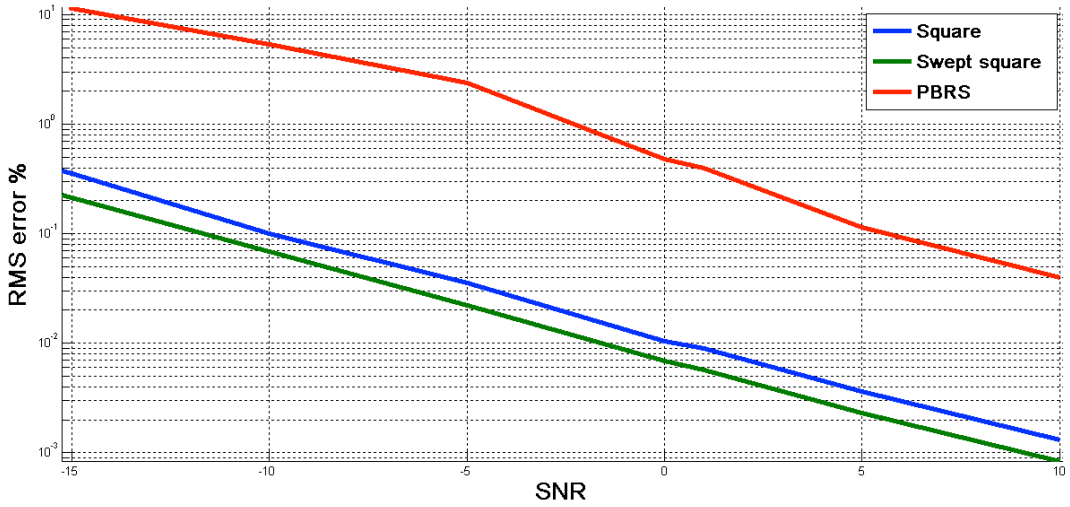

Figure 11. Mean squared estimation error in % for different output SNR - average value taken over 100 noise realizations.

IV. EXPERIMENTAL RESULTS

A. Hardware and implementation

The work was realized on a graphite/LiFePO4 cell with a nominal capacity of 2.3 Ah (ANR26650m1 battery from A123 Systems Company Ltd). To evaluate the performance of broadband signals for the identification of this battery impedance, experiments have been carried out at room temperature under the same operating conditions as those taken during simulations (SOC of 60% and DC current of 1A, number of blocks L=2059, T=0.0769s). A sampling frequency of 10240 Hz was used because of experimental device constraints so that the block size in samples was set to N=787 in order to obtain the same time duration T as in simulations. An electronic circuit was designed to perform the experiments and to allow application of input current with squared patterns, particularly swept square and PRBS. The acquisition of the input current and the corresponding output voltage response has been performed with an important SNR level thanks to an OR-36, a high performance acquisition device (24 bits).

During each experiment, three consecutive realizations of a single excitation signal (3*2059 blocks) are applied to study the variability of the estimation. It should be noted that such solicitation with a polarization current of 1A affects the SOC during the test (in the order of 6%) and may thus disrupt the conditions under which the battery can be approximated by a LTI system. However referring to the experiments in [37], within the SOC interval [50% ,

60%] we can assume that the impedance is quite constant. Coherence information will be studied to verify this last assumption.

B. Experimental results

1) PRBS

During the first experiment, a PRBS is used as the input current. The corresponding estimated coherence is plotted in Figure 13, while Figure 15 shows the estimated electrical impedance. The coherence is clearly close to 1 all over the specified frequency band. This shows that the battery can be considered as a LTI system under these operating conditions, and that its electrical impedance will be correctly estimated. It can also be noticed that as shown by simulations of section III., the use of a PRBS current induces a decrease in the coherence near the upper limit frequency $f_{\max}$. This is also visible in Figure 15, where the variability of the estimated impedance with the different realizations is very small all over the frequency band, unless near the upper frequency.

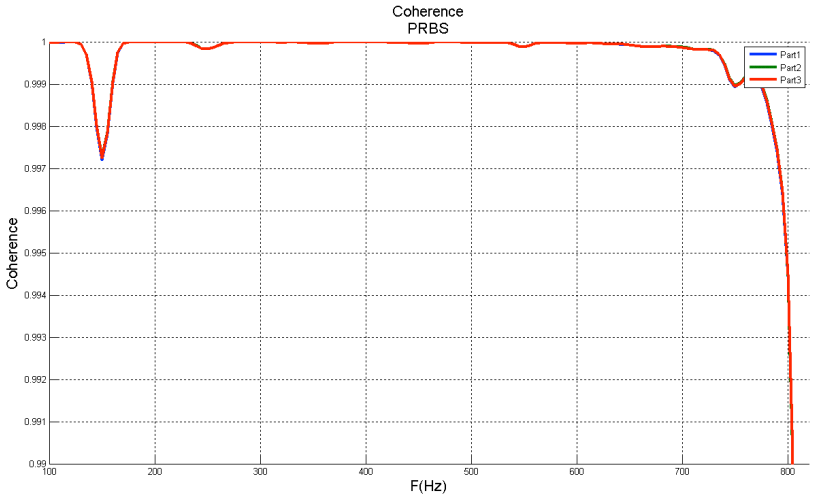

Figure 13. PRBS experimental results: coherence estimated for three measurements.

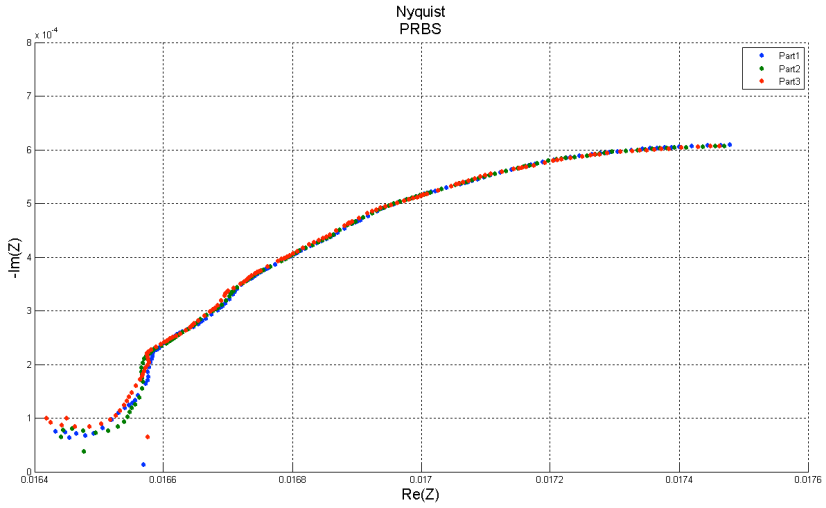

Figure 15. PRBS experimental results: complex-valued impedance estimated for three measurements.

2) Swept square

The input current during the second experiment is a swept square signal. Figure 17 and Figure 19 respectively show the corresponding estimated coherence and electrical impedance. As predicted in section III., this particular input signal leads to higher coherence values and better estimation performance all over the frequency band.

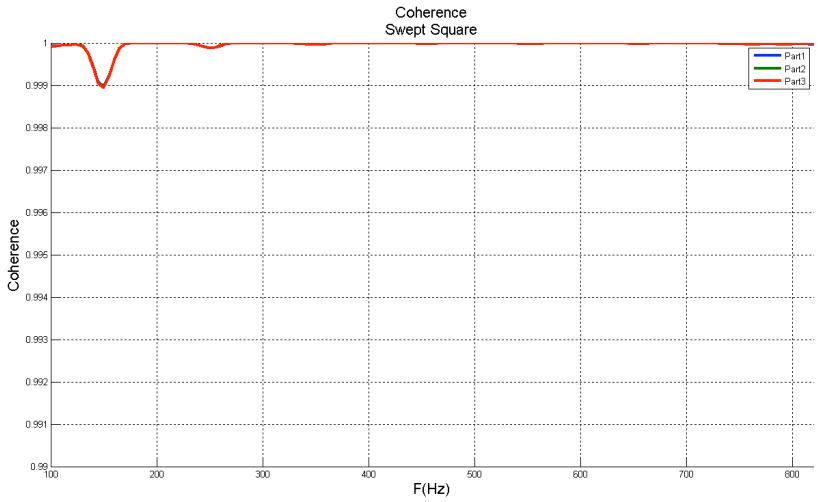

Figure 17. Swept square experimental results: coherence estimated for three measurements.

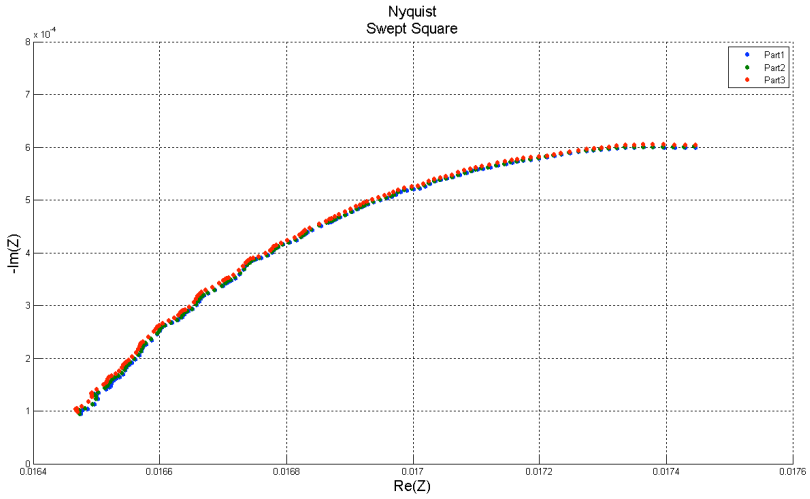

Figure 19. Swept square experimental results: complex-valued impedance estimated for three measurements.

Based on the high coherence values obtained during experiments, this battery can be considered as a LTI system within the chosen frequency band and under the chosen operating conditions. Moreover, confidence limits of impedance estimators are sufficiently small to affirm that the electrical impedance is accurately identified all over the frequency band, and that the swept square input current leads to better results than the PRBS.

V. CONCLUSION

This paper focuses on the usefulness of broadband excitation signals for the identification of a Li-ion battery electrical impedance. A non-parametric identification method has been theoretically introduced together with advanced parameters, such as spectral coherence function and confidence limits, able to evaluate the identification performance reached by this method. Simulation results indicate that identification patterns on input currents can be selected on the basis of their frequency characteristics, like power in the lowest frequencies of a selected band or flatness of their power spectral density over the whole band. This choice can be made by each user regarding the final use of the impedance measurement. Signals based on square pattern like swept square and PRBS lead to correct broadband identification, and are particularly well suited for electronic implementation. Experimental results ascertain the possibility to apply such a method to real batteries. Future works will focus on a comparative study to quantify the performance of the method by comparing it with standard electrical impedance spectroscopy in terms of precision, robustness, and computation time. A passive technique whithout the need to inject any additionnal current is a future line of research. () may be useful based on broadband identification technique.

REFERENCES

[1] Wakihara M. and Yamamoto O., (1998), *Lithium ion batteries: fundamentals and performance*, Wiley-VCH.

[2] Matsuki, K. and Ozawa, K., (2010), *General Concepts, in Lithium Ion Rechargeable Batteries: Materials, Technology, and New Applications* (ed K. Ozawa), Wiley-VCH VerlagGmbH & Co. KGaA, Weinheim, Germany. doi: 10.1002/9783527629022.ch1.

[3] Davide A., (ed) (2010), *Battery management systems for large Lithium-Ion battery packs*. Artech House, Boston – London.

[4] M. Doyle, T. F. Fuller, and J. Newman, (1993), *Modeling of galvanostatic charge and discharge of the lithium/polymer/insertion cell*, Journal of the Electrochemical Society, Volume 140, no. 6, p. 1526 – 1533.

[5] T. F. Fuller, M. Doyle, and J. Newman, (1994), *Simulation and optimization of the dual lithium ion insertion cell*, Journal of the Electrochemical Society, Volume 141, no. 1, p.1 – 10,.

[6] T. F. Fuller, M. Doyle, and J. Newman, (1994), *Relaxation phenomena in lithium-ion-insertion cells*, Journal of the Electrochemical Society, Volume 141, no. 4, p. 982 – 990.

[7] D. Rakhmatov and S. Vrudhula, (2001), *An analytical high-level battery model for use in energy management of portable electronic systems*, in Proceedings of the International Conference on Computer Aided Design (ICCAD'01), p. 488–493.

[8] C. Chiasserini and R. Rao, (1999), *Pulsed battery discharge in communication devices*, in Proceedings of the 5th International Conference on Mobile Computing and Networking, p. 88 – 95.

[9] C. Chiasserini and R. Rao, (1999), *A model for battery pulsed discharge with recovery e□ect*, in Wireless Communications and Networking Conference, p. 636 – 639.

[10] C. Chiasserini and R. Rao, (2001), *Improving battery performance by using tra□c shaping techniques*, IEEE Journal on Selected Areas in Communications, Volume 19, no. 7, p. 1385 – 1394.

[11] C. Chiasserini and R. Rao, (2001), *Energy e□cient battery management*, IEEE Journal on Selected Areas in Communications, Volume 19, no. 7, p. 1235 – 1245.

[12] Montaru M. Pelissier S., (2008). *Frequency and temporal identification of a Li-ion Polymer battery model using fractional impedance.* Les rencontres scientifiques de l'IFP - Advances in hybrid powertrains.

[13] Robinson R.S., (1993). System noise as a signal source for impedance measurements on batteries connected to operating equipment. Journal of Power Sources,Volume 2, p.365-368.

[14] Kozlowski J.D., (2003). *Electrochemical Cell Prognostics using Online Impedance Measurements and Model-Based Data Fusion Techniques*. Proceedings of the IEE Aerospace conference.Volume 7, p.3257-3270.

[15] J. Christophersen, D. Glenn, C. Motloch, R. Wright, C. Ho, and V. Bataglia, (2002) *Electrochemical impedance spectroscopy testing on the advanced technology development program lithium ion cells*, in Proc. IEEE 56th Trans. Veh. Technol., p. 1851–1855

[16] Ilangovan S.A., Sathyanarayana S., (1992). *Impedance parameters of individual electrodes and internal resistance of sealed batteries by non destructive technique*. Journal of applied electrochemestry,Volume 22, p.456-463.

[17] S.R Nelatury, P. Singh, (2002), *Extracting equivalent electric circuit parameters of lead acid cells from sparse impedance measurements*, Journal of Elsevier, Volume 112, p.621-625.

[18] Gregory L. Plett, (2004), *Extended Kalman filtering for battery management systems of LiPB-based HEV battery packs, Part 1. Background*, Journal of Power Sources, Volume 134, p. 252–261, 2004.

[19] Gregory L. Plett, (2004), *Extended Kalman filtering for battery management systems of LiPB-based HEV battery packs, Part 2. Modeling and identification*, Journal of Power Sources, Volume 134, p. 262–276.

[20] Gregory L. Plett, (2004), *Extended Kalman filtering for battery management systems of LiPB-based HEV battery packs, Part 3. State and parameter estimation*, Journal of Power Sources, Volume 134, p. 277–292.

[21] D.V. Do, C. Forgez, K. El Kadri Benkara, and G. Friedrich, (2009), *Impedance Observer for a Li-Ion Battery Using Kalman Filter*, IEEE TRANSACTIONS ON VEHICULAR TECHNOLOGY, Volume 58, no. 8.

[22] N. Watrin and *al.*(2012), *Multiphysical Lithium-Based Battery Model for Use in State-of-Charge Determination*, IEEE TRANSACTIONS ON VEHICULAR TECHNOLOGY, Volume 61, no. 8.

[23] Jonghoon Kim, B. H. Cho, (2011), *State-of-Charge Estimation and State-of-Health Prediction of a Li-Ion Degraded Battery Based on an EKF Combined With a Per-Unit System*, IEEE TRANSACTIONS ON VEHICULAR TECHNOLOGY, Volume 60, no. 9.

[24] P. Carbonini, T. Monetta, D.B. Mitton, F. Bellucci, P. Mastronardi, B. Scatteia,, (1997). *Degradation behaviour of 6013-T6, 2024-T3 alloys and pure aluminium in different aqueous media*, Journal of Applied Electrochemistry, Volume 27, p.1135-1142.

[25] L. Garrigues, N. Pebere, F. Dabosi, (1996). An investigation of the corrosion inhibition of pure aluminium in neutral and acidicchloride solutions, Electrochimica Acta, Volume 41, p.1209-1215.

[26] J.C. Uruchurtu, (1991). *Electrochemical investigations of the activation mechanism of aluminium*, Corrosion Volume 47, p. 472-479.

[27] S.C. Creason, J.W. Hayes, D.E. Smith (1973), *Fourier transform faradic admittance measurements II. Comparison of measurement efficiency for various test signal waveforms,* Journal of Electroanalytical chemistry and interfacial electrochemistry, Volume 47, p.9-46.

[28] C. Gbrielli (1992). *Comparison of sine wave and white noise analysis for electrochemical impedance measurements,* Electroanalytical Chemistry, Volume 335, p.33-53.

[29] G.S. Popkirov, R.N. Schindler (1993). *Optimization of the perturbation signal for electrochemical impedance spectroscopy in the time domain,* Volume 64, p.3111.

[30] Pintelon R., Schoukens J., (2001). *System identification, a frequency domain approach.* First Edition, IEEE press marketing, Piscataway,NJ (ISBN 0-7803-6000-1).

[31] Shin K., Hammond J.K., (Ed) (2008). *Fundamentals of Signal Processing for Sound and Vibration Engineers*. West Sussex PO19 8SQ, England.

[32] Bendat J.S., Piersol A.G. (2010). *Random data: analysis and measurements procedures*. Fourth Edition, John Wiley & Sons, Inc., Hoboken, NJ, USA

[33] Brillinger D. R. (2001). *Time Series: Data Analysis and Theory,* SIAM San Fransisco,USA.

[34] Halliday D.M, Rosenberg J.R al (1995). *A framework for the analysis of mixed time series/point process data-theory and application to the study of physiological tremor, single motor unit discharges and electromyograms*. ELSIVIER Science, Volume 64, No. 2/3, p.237-278.

[35] Jenkins G.M. and Watts D.G., (1968). *Spectral analysis and its applications.* Holden day, San Francisco, USA.

[36] Urbain M., (2009). *Modélisation électrique et énergétique des accumulateurs Lithium-Ion. Estimation en ligne du SOC et SOH*. Thesis, Institut National Polytechnique de Lorraine, France.

[37] Dong K., (2011). *Dynamic Modeling of Li-Ion Batteries Using an Equivalent Electrical Circuit.* Journal of the Electrochemical Society, Volume 158 (3), p.A326-A336.

[38] Wang X., Sone Y. and Sabura K. (2005). *Effect of operation conditions on simulated low-earth orbit cycle life testing of commercial lithium-ion polymer cell.* Journal of Power Sources, Volume142, p.313-322,

[39] Wu M.S., Chiang P.C and Lin J.C (2005). *Electrochemical investigations on capacity fading of advanced Lithium ion batteries after storing at elevated temperature*. Journal of Electrochemical Society, Volume 152, p.A1041-A1046.

[40] Ratnakumar B.V. and *al* (2004). *Behavior of li-ion cell in high intensity radiation environments*,Journal of Electrochemical Society, Volume 151, p.A652-A659

[41] Nagasubramanian G.(2000). *Two and three electrode impedance studies on 18650 Li-ion celles*, Journal of Power Sources, Volume 87, p.226-229.

[42] J.E.B. Discuss Faraday Society (1947), Volume1, p11

[43] Kuhn E., Forgez C. and Friedrich G., (2004). *Modeling diffusive phenomena using non integer derivatives.* The European Physical Journal Applied Physics, Volume 25, p.183-190.

[44] Oustaloup A., (1995). *La dérivation non entière : Théorie, Synthèse et Applications*, Editions Hermes.

[45] Oustaloup A., (2005). *Représentation et identification par modèle non entier*, Hermès Sciences.

[46] Wachtler M., Besenhard J.O and Winter M., (2001), *Tin and tin-based intermetallics as new anodematerials for lithium-ion cells*, Journal of Power Sources, Volume 94, p.189-193.

[47] Jeong S.K, Inaba M., Abe T. and Ogumi Z., (2001). *Surface film formation on graphite negative electrode in Lithium-ion batteries : AFM study in an ethylene carbonate-based solution*, Journal of Electrochemical Society, Volume 148, p.A989-A993.

[48] Buller S., (2002). *Impedance-Based Simulation Models for Energy Storage Devices in Advanced Automotive Power Systems*, Thesis, Institute for power electronics and electrical drives ISEA, Aachen/Germany.

[49] Buller S., Thele M., De Doncker A.W.AA and Karden Eckhard (2005). *Impedance-based simulation models of supercapacitors and Li-ion batteries for power electronic applications*, IEEE transactions on industry applications, Volume 41, p. 742-747.

[50] Buller S., Thele M., De Doncker A.W.AA and Karden Eckhard (2005), *Supercapacitors and lithium-ion batteries for power electronic applications*, IEEE Industry Applications Magazine, Volume11, p.62-67.

[51] Moss. P.L., Au G., Plichta E.J. and Zheng J.P., (2008) *An electrical circuit for modeling the dynamic response of li-ion polymer batteries,* Journal of Electrochemical Society, Volume 155, p.A986-A994.

[52] Al Nazer R., Cattin V., Granjon P. and Montaru M., (2012) *A new optimization algorithm for a li-ion battery equivalent electrical circuit identification*, 9th international conference of modeling, optimization and simulation (MOSIM 2012).

[53] Barsoukov, E. and Macdonald, J. R. (eds) (2005). *Frontmatter, in Impedance Spectroscopy: Theory, Experiment, and Applications*, Second Edition, John Wiley & Sons, Inc., Hoboken, NJ, USA

BIOGRAPHIES

R. AL NAZER received an engineering degree in electronics from Lebanese University-Faculty of Engineering. Then, she got a research master dispensation from the "Doctoral college of Grenoble Institute of Technology" and is currently pursuing the PHD degree at the CEA-LETI (Electronics and Information Technology Laboratory). Her recent interest is focused on impedance identification of the battery implemented in hybrid electric and electric vehicles.

CATTIN Viviane

After an engineering degree in electronics and signal processing and a PhD in signal image and speech processing, I work at the CEA since 1998 as a research engineer in the fields of detection and localisation from magnetometers and accelerometers, as a leader of industrial and collaborative projects on motion capture and drift measurement of cars. I supervised two PhDs and several students on signal processing, recently applied to battery diagnosis and monitoring. I am currently in charge of a laboratory working on advanced electronics for energy and power applications.

P. GRANJON received its PhD. degree from the Grenoble Institute of Technology (INPG), France in 2000. He joined the Laboratoire des Images et des Signaux (LIS) in 2002 and the Gipsa-lab at INPG in 2007, where he holds a position as associate professor. His current research is mainly focused on signal processing applications in diagnosis and electrical engineering, such as fault diagnosis in electrical systems, power networks, rotating machinery and batteries.

M. MONTARU received the Ph.D. degree from the Grenoble Institute of Technology (INPG), France in 2009. He joined the Electrical Storage Laboratory (LSE), where he holds a position as researcher engineer. His current research is mainly focused on battery behavior and ageing modeling in order to enhance battery states indicators and management.

M. RANIERI has been working since 2010 on BMS (Battery Management System) for electric vehicles. He is specialized in analog and digital electronic systems, especially for embedded applications, as well as in benchmark measurement systems. He works in Cea-Grenoble (France) in the DRT department (Technological Research) He has a master degree in electronic engineer. He is 33 years old.